sustainability

MDPI

Article

Optimization Strategy for Selecting the Combination Structure of Multilayer Phase Change Material (PCM) Glazing Windows under Different Climate Zones

Yao Lu [1,2], Faisal Khaled Aldawood [3], Wanyu Hu [1,2], Yuxin Ma [4], Mohamed Kchaou [3,*], Chengjun Zhang [1,2], Xinpeng Yang [1,2], Ruitong Yang [1,2], Zitong Qi [1,2] and Dong Li [1,2,*]

1 School of Architecture and Civil Engineering, Northeast Petroleum University, Fazhan Lu Street, Daqing 163318, China; luyao_300@163.com (Y.L.); huwanyu323@126.com (W.H.); 261993092011@nepu.com (C.Z.); yangxinpeng1996@163.com (X.Y.); rt_yang@stu.nepu.edu.cn (R.Y.); 13069616238@163.com (Z.Q.)
2 International Joint Laboratory on Low-Carbon and New-Energy Nexus, Northeast Petroleum University, Daqing 163318, China
3 Department of Mechanical Engineering, College of Engineering, University of Bisha, P.O. Box 001, Bisha 67714, Saudi Arabia; faldawood@ub.edu.sa
4 Beijing Key Laboratory of Green Built Environment and Energy Efficient Technology, Beijing University of Technology, Beijing 100124, China; mayuxin0110@163.com
* Correspondence: kchaou.mohamed@yahoo.fr (M.K.); lidong@nepu.edu.cn (D.L.)

Abstract: To improve the energy efficiency and photo-thermal performance of a double-layer PCM glazing window (DP), multilayer PCM glazing windows integrating DP (combination structures) with installations and low-e coating have been developed. However, the energy efficiency of a multilayer glazing window is not higher than DP in all climate zones. The selection of the appropriate optimization strategy of DP, i.e., selecting the most energy-saving multilayer glazing window, should take into account the specific climatic conditions. In this study, five PCM glazing windows (DP and four multilayer combination structures) are proposed. Physical heat transfer and mathematical models were conducted to numerically investigate the thermal and energy performance by Fluent in different climate zones in China. Evaluation indexes for different climate zones were established, and the energy-saving potential of each PCM glazing window was compared, and the resulting combination structure with the most energy-saving potential in each climate zone was regarded as the optimization strategy of DP. The results demonstrated that DP with the external silica aerogel has been identified as the optimization strategy for severe cold zones with 40.28% of energy saved, but it increases energy consumption in mild zones and hot summer and warm winter zones. DP with an external air layer and internal low-e coating is considered for the optimization strategies for cold zones, hot summer, and cold winter zones, and hot summer and warm winter zones, with energy-saving potential rates up to 40.67%, 46.42%, and 46.99% respectively. However, it increases energy consumption in mild zones and cold zones. In addition, DP is proven to possess the lowest energy consumption in mild zones.

Keywords: PCM glazing window; climate zones; optimization strategy; climate applicability; energy-saving potential

Citation: Lu, Y.; Aldawood, F.K.; Hu, W.; Ma, Y.; Kchaou, M.; Zhang, C.; Yang, X.; Yang, R.; Qi, Z.; Li, D. Optimization Strategy for Selecting the Combination Structure of Multilayer Phase Change Material (PCM) Glazing Windows under Different Climate Zones. *Sustainability* **2023**, *15*, 16267. https://doi.org/10.3390/su152316267

Academic Editor: George Kyriakarakos

Received: 27 October 2023
Revised: 15 November 2023
Accepted: 21 November 2023
Published: 24 November 2023

1. Introduction

Glazing windows are an essential part of building and play a vital role in sustainable development [1,2]. However, in comparison to other building envelopes, glazing windows have less thermal inertia, which results in more susceptible internal surface temperature fluctuations in the external environment [3]. Furthermore, glazing windows are responsible for a significant factor of energy consumption through buildings [4,5]. In view of this,

attention needs to be paid to the implementation of energy retrofit measures to enhance thermal performance for glazing windows [6].

Nowadays, phase change materials (PCMs) show their high potential for good heating storage and insulation effects in the field of energy-saving building and sustainable development [7–11]. The incorporation of PCMs into building envelopes as a means of thermal energy storage [12] optimizes indoor thermal comfort and improves the energy efficiency of buildings [13]. Therefore, it has been proposed to combine PCMs with glazing windows to improve the thermal performance of the traditional forms [14–16].

A large and growing body of literature has investigated a double-layer glazing window (DP) containing PCMs. In present studies, the performance of DP for solar photothermal utilization has been widely reported. Goia et al. [17,18] indicated that DP demonstrated impressive capabilities in superior thermal performance and solar energy storage. Bolteya et al. [19] indicated that DP could contribute to the thermal regulation of highly glazed buildings in the dry arid region of Egypt. Liu et al. [20] discovered that interreflections within windows during the phase change of PCMs lead to dynamic changes occurring in optical properties that negatively affect the heating transfer and thermal storage abilities of DP. The above references demonstrate that the thermal performance and energy efficiency of glazing windows can be effectively enhanced by filling PCMs. However, DP has limitations. Firstly, the melting process of PCMs is strongly affected by outdoor temperature and solar radiation, making them insufficient to cope with severe climate change, ultimately leading to increased energy consumption of buildings. Additionally, DP may limit solar heat gain to some extent due to the lack of regulation for different wavelengths of daylight spectrum. Therefore, in order to improve the thermal and energy performance of DP, it is crucial to improve the physical properties of PCMs filled in DP.

A number of combination structures have been proposed to improve the performance of the PCM layer [21]. With respect to the negative impact of outside factors on PCMs, many studies have delved into incorporating insulation in addition to PCMs. Li et al. [22] proposed a PCM glazing with an inside air layer, which showed an effective avoidance of overheating and a superiority in reducing inside surface temperature fluctuations and the heat entering the building in summer. Berthou et al. [23] and Souayfane et al. [24] introduced translucent passive solar walls consisting of a silica aerogel layer and a PCM glass bricklayer and showed that superior effectiveness during winter and transition seasons, but it may lead to overheating in summer.

With regard to the improvement of the radiation modulation ability of the PCM layer, incorporating nanofluids in PCMs is executable [25]. It can lead to a shorter phase transition time and an overall enhancement in light absorption properties [26]. However, the modification has two negative effects [27]. Firstly, the presence of nano-additive reduces the latent fusion heat of the matrix PCM, bringing about a significant energy density drop. Secondly, the synthesis of an ideal NPCM requires a higher cost [28]. Thus, complementing PCMs with reflective coatings that possess high solar reflectance and infrared emissivity can be considered [29]. Lei et al. [30] studied the use of cold-colored coatings in combination with PCMs in tropical climates and showed that the monthly cooling energy savings ranged from 5% to 12%. Ji et al. [31] combined thermochromic (TC) coatings with PCMs. By modulating the effect of solar radiation to improve PCM energy efficiency, they showed that the TC-PCM system can enhance the performance of PCMs, which can achieve the lowest annual energy demand in the climate of Shanghai.

The aforementioned studies demonstrate that PCMs in a composite structure with insulation and coating can optimize the utilization of latent heat within a specified range. The resulting composite structure outperforms DP in energy-saving in specific climate zones. This is due to the fact that the practical impact of PCMs [21], insulation [32], and coatings [33] on indoor thermal comfort and energy-saving potential is subject to different climatic conditions. For instance, Li et al. [34] found the energy performance of a hybrid PCM-containing wallboard (including three different PCMs) beneficial for buildings located in hot summer and cold winter zones but ineffective in hot summer and warm winter

zones. Wang et al. [35] found a roof-containing PCM with a reflective film performed better in the temperature climate with summer rain and the temperature climate with frequent rain areas. Several researchers [36–38] have concluded that aerogel glazing systems have a high energy-saving potential in severe cold zones and mild zones and are more suitable for cold zones and hot summer and cold winter zones. There are also studies showing that it is vital to take climate conditions into account when working with low-e materials, and significant differences in energy saving can be obtained between cold zones, hot zones, and warm summer and cold winter zones [39].

Furthermore, the five different climate zones in China have distinct varying demands for heating and cooling on buildings, necessitating strategies that can utilize or limit thermal gains and glazed structures with different needs. Therefore, in the process of structural design, the differences in climate zones should be fully considered in order to realize the ideal energy-saving state. Comparison of the energy-saving potential of each multilayer-PCM-glazed structure in different climate zones in China and the derivation of optimization strategies for DP applicable to the climate zone are essential for studying the feasibility and limitations of various PCM glazing windows across different climate zones and are informative for the promotion of PCM glazing windows in China.

According to the discussion above, this paper is to comprehensively investigate the thermal performance and energy-saving potential of five PCM glazing windows (DP, TAGP, TAEP, TPGA, and TSGP) appended to air, silica aerogel, and low- e coating. Furthermore, the outdoor temperature and solar radiation in each climate zone are analyzed, and the typical days simulated are selected based on average temperatures during heating or cooling periods. The phase-change temperatures of PCMs used in various climate zones vary and are determined based on indoor and outdoor temperatures during heating or cooling periods, which enables PCMs to fully utilize latent heat and optimize energy efficiency. Numerical simulations are carried out via Fluent to analyze the thermal performances of PCM glazing windows on a typical day. Formulas were then developed to calculate the adopted energy, and the evaluation indexes of energy-saving potentials were established to analyze the applicability of the five types of PCM-glazed structure in terms of the energy-saving rate and the thermal performance in five representative cities of different climate zones in China (Harbin, Beijing, Wuhan, Guangzhou, and Kunming). The resulting combination structure with the most energy-saving potential in each climate zone is regarded as the optimization strategy of DP. A comprehensive evaluation of different PCM-glazed structures in different climate zones can not only provide a theoretical basis for the selection but also establish frameworks for future research on a scientific and rational design and sustainable utilization of optimized structures for DP (Figure 1).

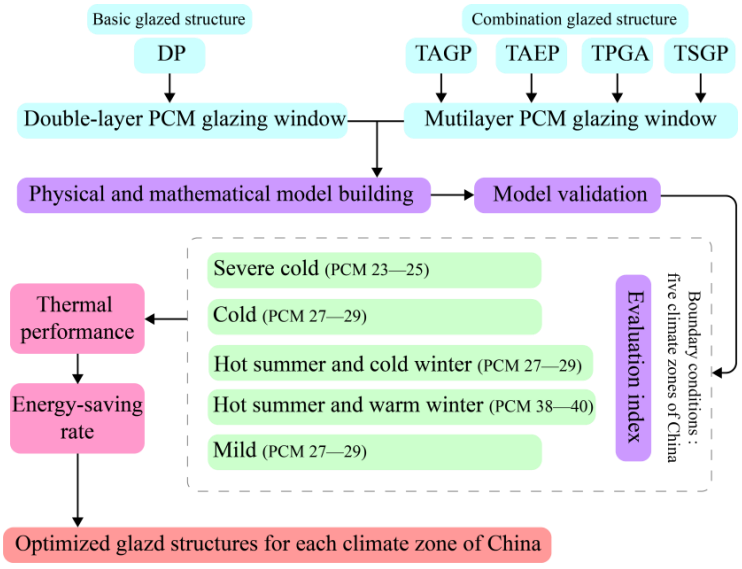

Figure 1. Workflow of the present work.

2. Methods

2.1. Physical Model

The physical models of PCM glazing windows studied are shown in Figure 2, where the double-layer PCM glazing window is designed as a contrast structure (4 + 6 + 4 mm), and the other four multilayer PCM glazing windows are multilayer optimized structures (4 + 6 + 4 + 6 + 4 mm) containing different material layers added to the contrast structure. The details of PCM glazing windows along with the thermal and optical parameters of materials are given in Tables 1 and 2, respectively.

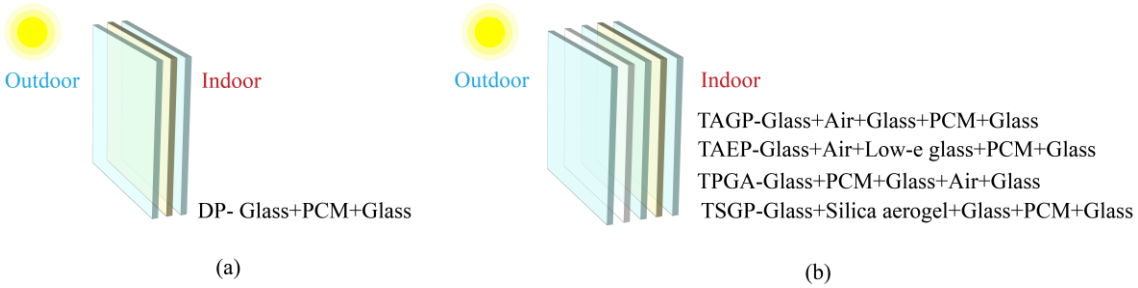

Figure 2. Structure of PCM glazing windows: (**a**) Double-layer PCM glazing window; (**b**) Multilayer PCM glazing window.

Table 1. Details of PCM glazing windows.

Glazing Windows	Construction (from Outside to Inside)
DP	6 mm Glass + 4 mm PCM + 6 mm Glass
TAGP	6 mm Glass + 4 mm Air + 6 mm Glass + 4 mm PCM + 6 mm Glass
TAEP	6 mm Glass + 4 mm Air + 6 mm Low-e glass + 4 mm PCM + 6 mm Glass
TPGA	6 mm Glass + 4 mm PCM + 6 mm Glass + 4 mm Air + 6 mm Glass
TSGP	6 mm Glass + 4 mm Silica aerogel + 6 mm Glass + 4 mm PCM + 6 mm Glass

Table 2. Thermal and optical parameters of materials. Thermal and optical parameters of traditional glass, low-e glass, and silica aerogel.

Materials	λ (W/(m·°C))	c_p (J/kg·°C)	ρ (kg/m^3)	n	α (1/m)
Traditional glass	0.96	840	2500	1.5	19
Low-e glass [40]	0.96	840	2500	0–2.5 μm 1.5 2.5–∞ μm 10	2.5–∞ μm 12 2.5–∞ μm 3.4
Silica aerogel [24]	0.018	1500	100	1.01	12
Thermal and optical parameters of PCM.					
PCM	**λ (W/(m·°C))**	**c_p (J/kg·°C)**	**ρ (kg/m^3)**	**n**	**α_s/α_l (1/m)**	**Q_L (kJ)**
PCM 23–25	0.25	2230	890	1.3	80/20	185,000
PCM 27–29	0.21	2230	850	1.3	80/20	205,000
PCM 38–40	0.225	2230	892	1.3	80/20	174,000

The heat transfer process is shown in Figure 3. The solar radiation incident on glazing windows is reflected, transmitted, and absorbed by glazing windows, respectively. There are two parts to the absorbed solar radiation heat: partly transferred to the room by the glazing windows in the form of convective and radiant heat exchange with the indoor environment and partly stored in the inner structural layers of glazing windows.

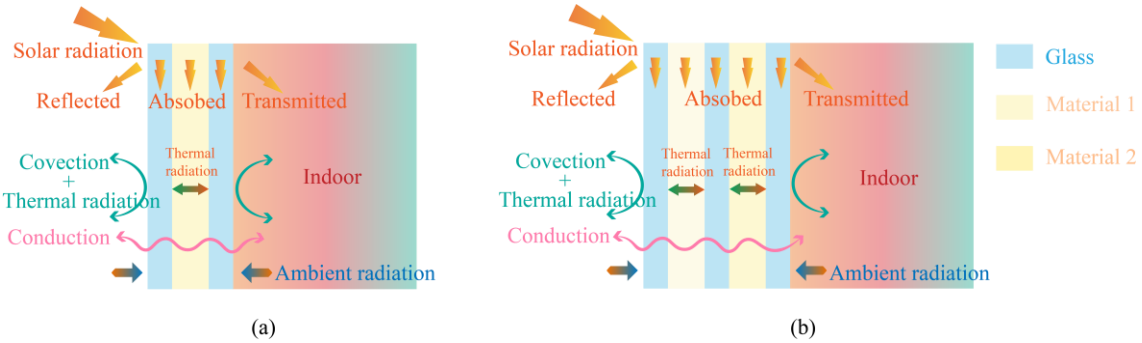

Figure 3. Heat-transfer mechanism of PCM glazing windows: (**a**) Double-layer PCM glazing window; (**b**) Multilayer PCM glazing window.

2.2. Climate Zones of Five Representative Cities in China

According to the Code for the Thermal Design of Civil Buildings [41], China is divided into five typical climate zones, including severe cold, cold, hot summer and cold winter, hot summer and warm winter, and mild zones (Figure 4). Harbin is a representative city in the severe cold zone, located at 126°63′ E and 45°75′ N. Its climate is mid-temperate continental monsoon, characterized by cold and lengthy winters that entail significant building energy consumption for heating. Beijing is a city in the cold zone, situated at 116°20′ E and 39°56′ N. It experiences a warm temperate semi-humid and semi-arid monsoon climate with cold winter and high summer. Therefore, the energy consumption of buildings during the heating and cooling periods is vital for study. Wuhan, representing the hot summer and cold winter zone, is located at 114°32′ E and 30°52′ N. It has a subtropical monsoon climate with cold winter and hot summer, and the energy consumption of buildings during heating and cooling periods must be taken into consideration. Guangzhou, representative of the hot summer and warm winter zone, is located at 113°23′ E and 23°17′ N, with a subtropical monsoon climate. Here, building energy consumption accounts for most of the cooling period. Kunming, located at 25°02′ N and 102°42′ E, is a prominent city in the mild zone. It has a subtropical highland monsoon climate with four seasons like spring and mild weather. However, the daily temperature difference in winter can reach 12–20 °C, necessitating the consideration of building energy consumption during the heating period.

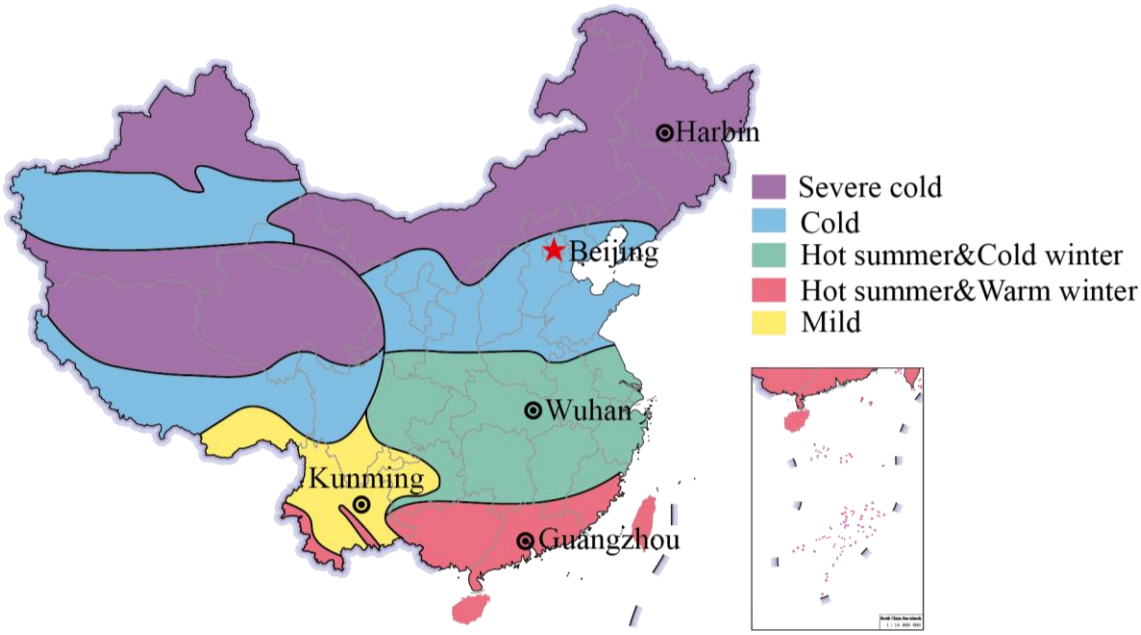

Figure 4. China climate zones.

The heating and cooling periods of each city are defined according to the Special Meteorological Data Set for Building Thermal Environment Analysis in China and the specific policies of municipal governments [42]. For reliability and validity, the simulated typical days are selected based on the average temperature of heating or cooling periods, and the daily average temperature and maximum horizontal solar radiation values of the typical days are shown in Table 3. CSWD meteorological data on hourly temperature and hourly horizontal solar radiation taken for this study are obtained from Energy Plus meteorological data [43].

Table 3. The heating period and cooling period of representative cities in each climate zone.

Representative City	Climate Zone	Heating Period	Cooling Period	PCM Melting Temperature (°C)
Harbin	Severe cold	20 October–20 April next year	-	23–25
Beijing	Cold	15 November–15 March next year	1 June–15 September	27–29
Wuhan	Hot summer and cold winter	15 November–15 March next year	15 May–15 September	27–29
Guangzhou	Hot summer and warm winter	-	15 May–15 October	38–40
Kunming	Mild	15 November–15 March next year	-	27–29

2.3. Mathematical Model

On the premise that physical models keep precision, in order to give prominence to heat transfer processes, the numerical procedure of multilayer PCM glazing window models is aimed to simplify. The following assumptions are made:

(1) Only the height and thickness of glazing windows are considered, and the heat transfer process is considered a two-dimensional unsteady state.
(2) The effect of window frames on the heat transfer process is ignored. The upper and lower walls and the remaining surfaces of glazing windows are determined to be adiabatic and conjugate heat transfer boundary conditions, respectively.
(3) All materials in glazing windows are considered isotropic, and the heat transferred and solar radiation absorbed during the heat transfer process are considered uniformly distributed.
(4) The absorption coefficients for solid and liquid phases of the same phase change material are different constants, and the rest of the physical parameters of the material are fixed values.

2.3.1. Governing Equations

As depicted in Figure 2, a double-layer or multilayer PCM glazing window comprises regions consisting of glass, air, silica aerogel, and PCM layers. The un-stationary heat transfer equation for the glass, air layer, and silica aerogel layer is expressed as follows:

$$\rho c_p \frac{\partial t}{\partial \tau} = \lambda \frac{\partial^2 t}{\partial x^2} + \lambda \frac{\partial^2 t}{\partial y^2} + \phi \quad (1)$$

where λ is thermal conductivity, W/(m·K); ρ is density, kg/m^3; c_p is specific heat, J/(kg·K); t is temperature, K; τ is time, s; ϕ is the source term from solar radiation, W/m^3, which can be established by:

$$\phi = \int_{\Omega_{i=4\pi}} I\left(\vec{r}, \vec{s}\right) \Omega d\Omega_i \quad (2)$$

where $I(\vec{r}, \vec{s})$ is radiation intensity, W/m^2; and are position and direction vectors.

The transfer of solar radiation through a multilayer PCM glazing window is shown below [44]:

$$\frac{dI\left(\vec{r},\vec{s}\right)}{ds} = \alpha n^2 \frac{\sigma T^4}{\pi} - \alpha I(\vec{r},\vec{s}) \tag{3}$$

where α is the absorption coefficient of the transparent medium layer, 1/m; σ is the Stefan-Boltzmann constant.

For the PCM layer, the un-stationary heat transfer equation is given by the following equation:

$$\rho \frac{\partial H}{\partial \tau} = \lambda \frac{\partial^2 t}{\partial x^2} + \lambda \frac{\partial^2 t}{\partial y^2} + \phi \tag{4}$$

where H is specific enthalpy (kJ/kg), which can be established by:

$$\begin{array}{l} H = \int_{t_0}^{t} c_p dt + \varphi Q_L \\ \varphi = \frac{t-t_m}{t_m-t}, t_m \le t \le t_s \\ \varphi = 0, t < t_m \\ \varphi = 1, t > t_s \end{array} \tag{5}$$

where t_0 is the standard temperature, and t_m and t_s are the initial melting and solidification temperature of PCM, respectively, K; φ is the fraction of liquid present during the transition from liquid to solid phases; Q_L is the latent heat, kJ/kg.

2.3.2. Boundary Equations

The physical models of multilayer PCM glazing windows include upper and lower wall adiabatic boundaries, and outside and inside surface boundaries of glazing windows.

The equation of upper and lower wall adiabatic boundaries:

$$-k \frac{\partial t}{\partial x} \| _{y=0} = 0 \tag{6}$$

$$-k \frac{\partial t}{\partial x} \| _{y=y_h} = 0 \tag{7}$$

where y_h is the height of the glazing window, m.

The outside and inside surfaces of the glazing window are subjected to radiation and heat conduction with the surrounding environment, where the heat balance equation for the outside surface of the glazing window is:

$$-k \frac{\partial t}{\partial \mathrm{y}} \| _{x=x_L} = I_{out} + h_0 (t_{out} - t_e) \tag{8}$$

where x_L is the thickness of the glazing window, m; h_0 is the heat transfer coefficient on the outside boundary, W/(m^2·K); t_{out} is outside boundary temperature, K; t_e is outdoor environment temperature, K; I_{out} [45] is the total radiation heat flux from the outside boundary to the ambient, which can be expressed as follow, W/m^2:

$$I_{out} = I_a + I_s + I_g \tag{9}$$

where I_a, I_s, and I_g, respectively, denote the heat radiation flux from the outside boundary to the atmosphere, sky, and ground.

The equation that defines the boundary inside the glazing window can be expressed as [46]:

$$-k \frac{\partial t}{\partial \mathrm{y}} \| _{x=0} = I_{in} + h_i (t_{in} - t_{e,i}) \tag{10}$$

where h_i is the heat transfer coefficient on the inside boundary, W/(m^2·K); t_{in} is inside boundary temperature, K; $t_{e,i}$ is indoor environment temperature, K; I_{in} is the total radiation

heat flux from the inside boundary to the indoor ambient, which can be expressed as follow, W/m^2;

$$I_{in} = \varepsilon\sigma\left((t_{in} + 273.15)^4 - (t_{e,i} + 273.15)^4\right) \tag{11}$$

where ε is the surface emissivity of the external glass layer.

2.4. Evaluation Index

The evaluation criteria were established using the cumulative hourly heat transfer through multilayer PCM glazing windows and the corresponding energy-saving rate. A comprehensive evaluation of climatic suitability and potential for energy-saving was conducted after analyzing the thermal performance of each glazing window and its impact on PCM layers.

Section 2.2 points out that for the severe cold and mild zones, the cumulative hourly heat of the heating period can be evaluated independently, while for the hot summer and warm winter zones, only the cumulative hourly heat of the cooling period needs to be considered. However, for areas like the cold zones and hot summer and cold winter zones that require both heating and cooling, a compromise must be made between the cumulative hourly heat of the heating and cooling periods. To conduct numerical simulations, a typical day with a daily mean temperature equal to the average temperature of the heating and cooling period was selected. Therefore, the algebraic sum of the cumulative hourly heat of heating and cooling periods can be considered as an approximate overall cumulative hourly heat for the area.

The cumulative hourly heat is calculated from the inside surface heat flux, which is given by the following equations.

Cumulative hourly heat of heating periods:

$$Q_h = \frac{60}{1000}\sum_{i=1441}^{2880} q_{i,h} \tag{12}$$

Cumulative hourly heat of cooling periods:

$$Q_c = \frac{60}{1000}\sum_{i=1441}^{2880} q_{i,c} \tag{13}$$

where Q_h and Q_c are the cumulative hourly heat through glazing windows during heating and cooling periods, respectively, kJ/(m^2·d); $q_{i,h}$ and $q_{i,c}$ are the inner surface heat flux of each time step, respectively, $q_{i,h}$ or $q_{i,c} > 0$ means heat flux from indoor to outdoor, and $q_{i,h}$ or $q_{i,c} < 0$ means heat transfer from outdoor to indoor, W/m^2; $\sum_{i=1441}^{2880} q_{i,h}$ or $\sum_{i=1441}^{2880} q_{i,c}$ is the algebraic sum of $q_{i,h}$ or $q_{i,c} < 0$ with the time step from 1441 to 2880 when the time step size is 60 s and the number of the time step is 2880 during the simulation, which is the total heat flux on the second computing day.

The transmittance of the models of glazing windows is computed via Equation (14) [19,47]:

$$\begin{aligned} \tau_m &= \frac{(1-\omega_i)\left(1-\omega_j\right)\exp(-\alpha_m d_m)}{1-\omega_i\omega_j\exp(-2\alpha_m d_m)} \\ w_{i,j} &= \frac{(n_i-n_j)^2}{(n_i+n_j)^2} \end{aligned} \tag{14}$$

where m represents various types of medium layers, including glass, silica aerogel, and PCMs; τ_m is transmittance, %; d_m is the thickness of each layer, m; i and j are the adjacent intermediate layers; $\omega_{i,j}$ is the interface reflectance obtained through Fresnel's equations; n is the refractive index.

Some of the solar radiation energy transmitted through glazing windows into the room is shown below:

$$\begin{aligned} \tau &= \tau_{m1} \times \tau_{m2} \times \cdots \times \tau_{mn} \\ E_\tau &= \tau \times I \end{aligned} \tag{15}$$

where m_1–m_n are the numbers of material layers; E_τ is the transmitted energy in solar radiation; I is the solar radiation energy of the selected typical day.

Cumulative hourly heat of severe cold zones, mild zones, and hot summer and warm winter zones:

Q during heating periods:

$$\begin{array}{l} Q = E_\tau + |Q_h|, Q_h < 0 \quad (a) \\ Q = E_\tau - Q_h \ , Q_h > 0 \quad (b) \end{array} \tag{16}$$

where Q is the total cumulative hourly heat through glazing windows, kJ/(m^2·d). When $Q_h < 0$, it indicates that energy from outdoors flows to indoors. Conversely, when $Q_h > 0$, it means that heat energy from indoors flows to outdoors. For both of them, the higher the value, the more efficient the building is in terms of energy consumption.

Q during cooling periods:

$$\begin{array}{l} Q = E_\tau + |Q_c|, Q_c < 0 \quad (a) \\ Q = E_\tau - Q_c \ , Q_c > 0 \quad (b) \end{array} \tag{17}$$

where Q is the total cumulative hourly heat through glazing windows, kJ/(m^2·d). When $Q_c < 0$, it indicates that energy from outdoors flows to indoors. Conversely, when $Q_c > 0$, it means that heat energy from indoors flows to outdoors; the smaller the number, the more efficient the building is in terms of energy consumption.

Cumulative hourly heat of the cold zone and hot summer and cold winter zone:

$$\begin{array}{ll} Q = (E_{\tau,c} + D_c|Q_c|) - (E_{\tau,h} + D_h|Q_h|), & Q_h < 0, Q_c < 0 \quad (a) \\ Q = (E_{\tau,c} - D_cQ_c) - (E_{\tau,h} + D_h|Q_h|), & Q_h < 0, Q_c > 0 \quad (b) \end{array} \tag{18}$$

where Q is the total cumulative hourly heat through glazing windows, kJ/m^2; D_c and D_h are the numbers of days during the cooling and heating periods, respectively, d. In both cases, the lower the Q value, the better the building's energy efficiency.

$$\begin{array}{ll} Q = (E_{\tau,c} + D_c|Q_c|) - (E_{\tau,h} - D_hQ_h), & Q_h > 0, Q_c < 0 \quad (a) \\ Q = (E_{\tau,c} - D_cQ_c) - (E_{\tau,h} - D_hQ_h), & Q_h > 0, Q_c > 0 \quad (b) \end{array} \tag{19}$$

where Q is the total cumulative hourly heat through the glazing window, kJ/m^2. In both situations, a lower Q value indicates greater energy efficiency for the building. This study discusses and gives the formula for the energy-saving rate, which is obtained by comparing the cumulative hourly heat of the multilayer-optimized structures and the contrast structure.

The energy-saving rate of the severe cold zone and mild zone:

$$r = \frac{Q_M - Q_D}{Q_D} \times 100\%, \quad Q_D < Q_M \tag{20}$$

The energy-saving rate of the cold zone, hot summer and cold winter zone, and hot summer and warm winter zone:

$$r = \frac{Q_D - Q_M}{Q_D} \times 100\%, \quad Q_M < Q_D \tag{21}$$

where r is the energy-saving rate of the multilayer PCM glazing window, %; Q_D is the heat through the basic structure, Q_M is the heat through the multilayer-optimized structure, which are both derived from Equations (16)–(19), kJ/(m^2·d).

2.5. Simulation Details and Model Validation

The thermal performance of multilayer PCM glazing windows is calculated and analyzed by Fluent (Ansys 2021 R1), and the models of entire glazing windows are established

and meshed using Design Modeler and Mesh (Ansys 2021 R1). All the computational equations of numerical calculation were carried out using the finite volume method, the second-order windward format, and the SIMPLE algorithm. In the simulation process, the indoor thermal comfort temperatures for heating and cooling periods were set to 18 °C (291.15 K) and 26 °C (299.15 K), respectively. In particular, the internal and external surface flow heat transfer coefficients were set at 7.43 W/m^2 and 7.75 W/m^2. And adopted to improve the efficiency and accuracy of calculation, the calculated data of the second day were selected for this study.

Model validation simulations were performed under the conditions of outdoor temperature and radiation parameters and physical parameters of the glazing windows established in the literature [48] to verify the reliability of the model and the accuracy of mesh quality. A comparison of the results and the simulated internal surface temperature results with experimental data in the literature [48] is shown in Figure 5. It displays that the average relative error is 4.4%, which is inferred from the model's modeling and solution method that is applicable to this study of the thermal performance of multilayer PCM glazing windows.

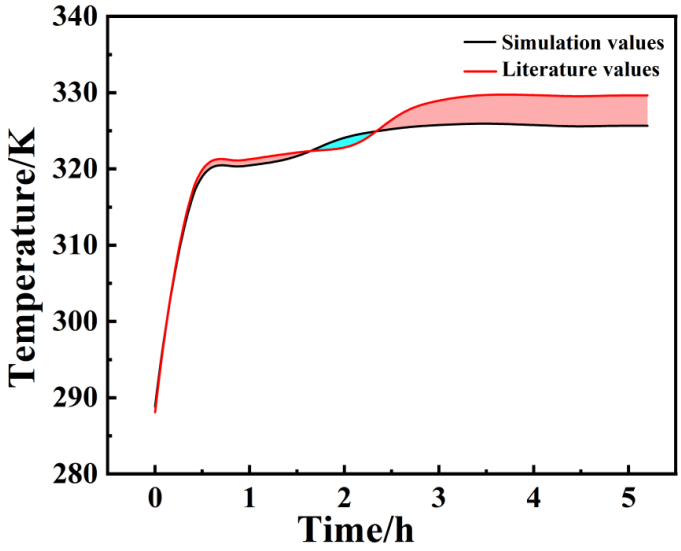

Figure 5. Verification of inner surface temperature of the double-layer PCM glazing window (blue zone corresponds to the literature values down the simulation values).

3. Results and Discussion

In this section, the thermal performance and suitability of five PCM glazing windows in five different cities of China are evaluated for the major energy consumption periods (heating and cooling). The thermal performance is characterized by examining variations in the liquid fraction of PCMs, interior surface temperature, and heat flux over time. The results of the climate suitability analysis are reflected through the cumulative heat passing through windows as well as the energy-saving rates.

3.1. Severe Cold Zone

The main consideration in severe cold zones is energy consumption during heating periods. As depicted in Figure 6, the environmental conditions outside in Harbin on 23 March were chosen to simulate the data, with a daily average temperature of 264.9 K and maximum solar radiation of 818 J/m^2. The daylight lasts from 7 a.m. until 6 p.m. The indoor temperature was set at 291.15 K.

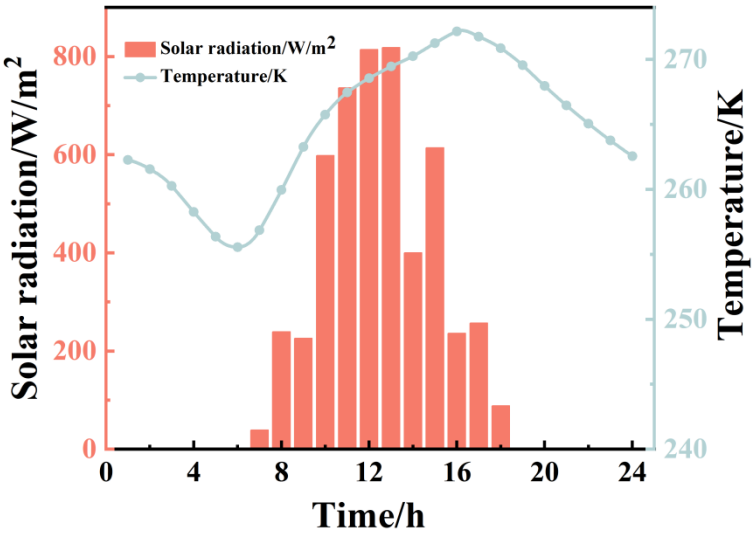

Figure 6. Hourly values of air temperature and solar radiation in Harbin.

The average liquid fraction of PCMs, variation in interior surface temperatures, and heat flux for glazing windows are depicted in Figure 7a–c. The fluctuation of temperature on the glazing window's inner surface and the time-to-temperature peak are shown in Table 4. It highlights that the combination structures lead to smoother and less drastic changes in ratio when compared to DP. It substantiates that the combination structures effectively mitigate the effects of indoor fluctuations in DP. These findings indicate the superiority of optimized structures over DP in reducing the impact of indoor fluctuations. Notably, TAEP exhibits the smallest deviation from the original trend.

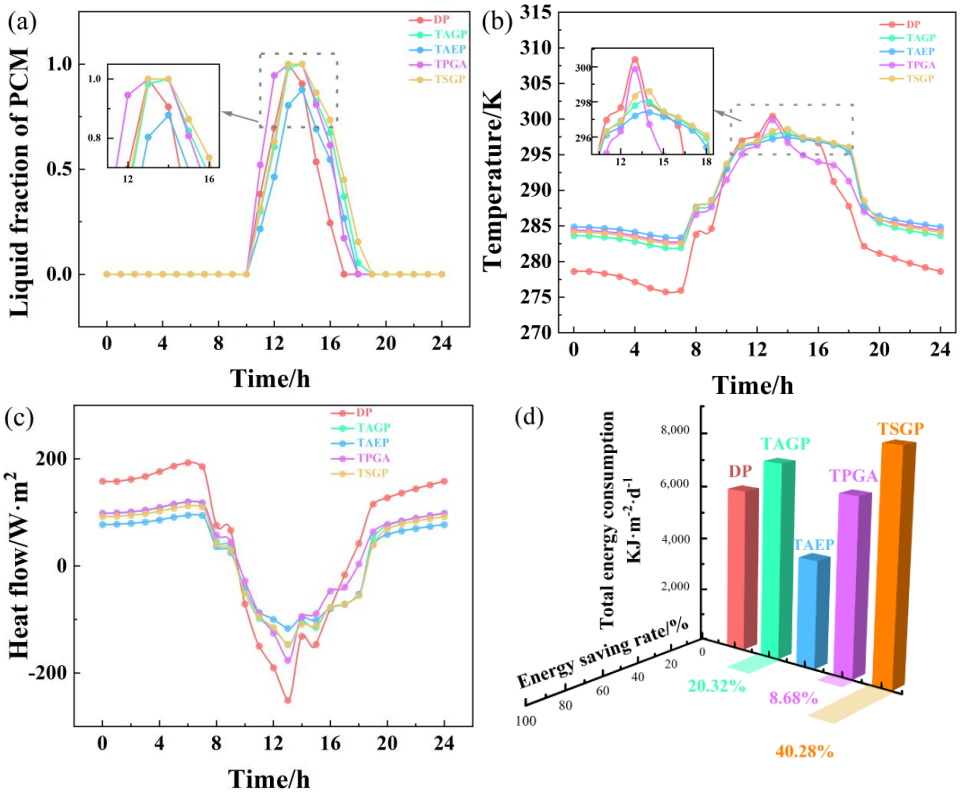

Figure 7. Thermal performance and energy efficiency of five glazing windows in severe cold zone: (**a**) Average liquid fraction of PCMs; (**b**) Average inner surface temperature; (**c**) Inner surface heat flow; (**d**) Total heat loss and energy-saving rate.

Table 4. Interior surface temperatures of different glazing windows and total energy entering the room through the glazing windows in Harbin (severe cold zone).

Glazing Window	Peak Value T_{max} (K)	Peak Time (h)	Valley Value T_{min} (K)	ΔT (K) = $T_{max} - T_{min}$	Average Value (K)	Q (kJ/(m^2·d))
DP	300.76	13.17	275.69	25.07	285.37	6076.40
TAGP	299.72	13.48	281.85	17.86	288.90	7311.36
TAEP	297.43	13.73	283.33	14.10	289.42	4039.24
TPGA	299.91	13.10	282.74	17.17	288.53	6603.68
TSGP	300.44	13.45	282.48	17.96	289.35	8524.07

As illustrated in Table 4, during the heating period in severe cold zones, energy flows from interior to exterior through glazing windows, as indicated by $Q_h > 0$. This situation is not favorable for indoor heating. Equation (16) can be used to calculate Q, which indicates that the higher the Q, the greater the heat gain in the room and the more potential for energy-saving. Figure 7d demonstrates Q and r, where TSGP exhibits the highest heat gain of 6076.40 kJ/(m^2·d), whereas TAEP presents a heat gain that is 2037.16 kJ/(m^2·d) lower than DP due to the implementation of low-e glass. The energy-saving rate of glazing windows can be determined using Equation (20). Remarkably, the energy-saving rate of TSGP can reach 40.28%, while that of TAGP can reach 20.32%, that of TPGA is 8.68%, and TAEP consumes a higher amount of heating energy compared to DP. It is attributed to the silica aerogel's high solar radiation absorption in TSGP, which enhances its heat radiation efficiency in the room as compared to other glazing windows. Furthermore, the extremely low thermal conductivity of silica aerogel mitigates the heat loss of TSGP at night, making it more energy-efficient than other optimized structures in severe cold zones.

What is indicated from the above findings is that to achieve energy saving, external insulation is more effective than internal insulation for DP located in severe cold zones. Additionally, silica-based insulation is found to be more efficient than air-based insulation. In contrast, incorporating low-e glass decreases the energy efficiency of DP, mainly due to its high reflectivity towards solar radiation. The optimization strategy for the combination of DP structures in severe cold zones is TSGP.

3.2. Cold Zone

Due to the need for both winter heating and summer cooling in Beijing, energy consumption should be considered for both heating and cooling periods. As depicted in Figure 8a, heating period environmental conditions outside Beijing on 24 February were chosen to simulate the data, with a daily average temperature of 272.9 K and maximum solar radiation of 822 J/m^2. The daylight lasts from 8 a.m. until 6 p.m. The indoor temperature was set at 291.15 K. And cooling period environmental conditions outside Beijing on 7 August were chosen to simulate the data, with a daily average temperature of 298.1 K and maximum solar radiation of 849 J/m^2. The daylight lasts from 7 a.m. until 8 p.m. The indoor temperature was set at 299.15 K.

Figure 9a–c and (1–3) depict trends in the liquid fraction of the PCM layer, the temperature, and the heat flux on the inner surface of the glazing windows during the heating and cooling periods, respectively. As can be seen from Figure 9a, TPGA has a maximum liquid phase rate of 0.87, and the phase transition takes place from 13:00 to 17:00. DP's rate is 0.56, while the rest structures have smaller liquid fractions and last 2 h. It suggests that during heating periods, when outdoor temperatures are low and solar radiation is at its peak, the PCM partially melts in cold zones. Adding insulation inside is more conducive to liquefying the PCM layer than adding it outside. Meanwhile, incorporating low-e glass reflects some of the solar radiation, thereby reducing PCM's absorption of solar energy and its liquefaction rate. As shown in Figure 9b, the maximum inner surface temperatures for all structures plateau at 14:00 with the same trend. Among all the structures, TPGA exhibits the lowest maximum inner surface temperature of 297.41 K from the inner surface and remains consistent across all structures, with TPGA and TAEP exhibiting the smoothest patterns.

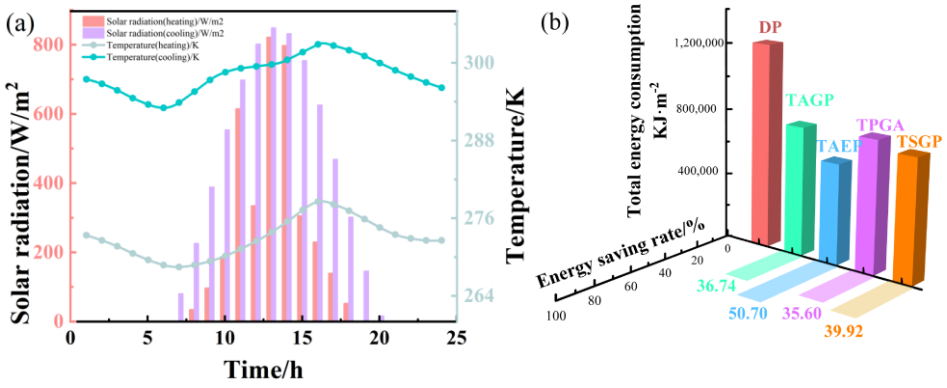

Figure 8. (**a**) Hourly values of air temperature and solar radiation in Beijing; (**b**) Total heat loss and energy-saving rate.

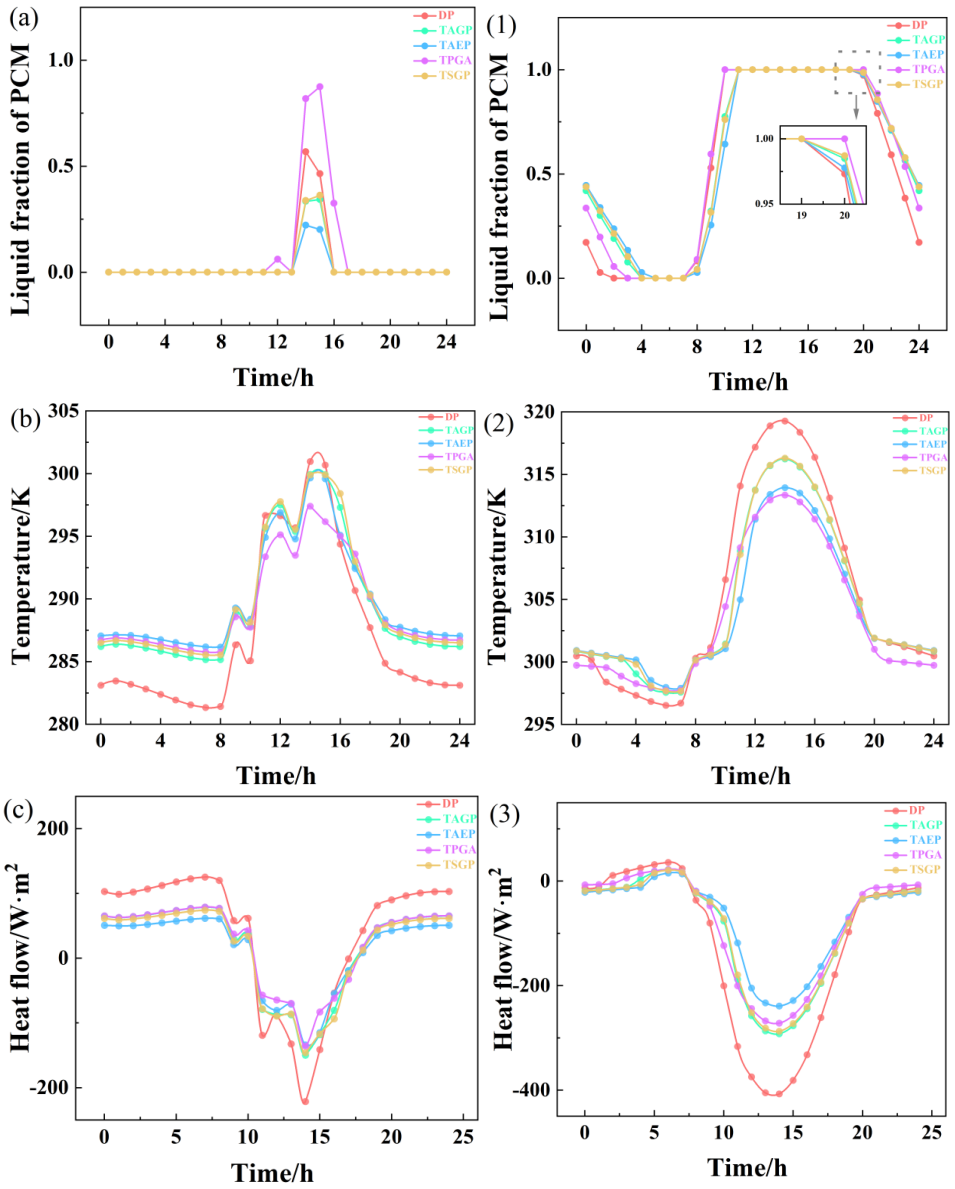

Figure 9. Thermal performance and energy efficiency of five glazing windows: Heating period in cold zone: (**a**) Average liquid fraction of PCM; (**b**) Average inner surface temperature; (**c**) Inside surface heat flow. Cooling period: (**1**) Average liquid fraction of PCM; (**2**) Average inner surface temperature; (**3**) Inner surface heat flow.

Considering the climatic characteristics of cold zones and the needs of the occupants of the building's indoor thermal environment, its cooling period should also be analyzed and discussed. As depicted in Figure 9(1), the PCM layers in all glass structures were completely melted. DP takes 10 h to fully liquefy, from 10:00 to 19:00. While TAGP, TAEP, and TSGP take 8 h to melt, from 12:00 to 20:00. TPGA takes 11 h to liquefy, from 10:00 to 21:00. It suggests that incorporating insulation on the outside of DP can decrease the time required for complete liquefaction of PCM layers and also mitigate overheating caused by PCMs melt in cold zones. Figure 9(2) shows that all glazing windows reach their maximum temperature at 15:00, with TPGA having the smallest inner surface maximum at 313.35 K, and its daytime temperature is closest to the desired indoor comfort temperature. In cold zones, adding insulation to the interior of DP during the cooling period can effectively block heat transfer from the PCM layer to the interior. TAEP comes in second. TAGP and TSGP can reduce some of the outdoor temperatures that enter the interior. However, since the PCM layer is placed inside, it can cause the PCM superheated temperature to dissipate directly to the interior. Figure 9(3) exhibits that heat flux through TAEP is the most consistent.

When applying Equations (12) and (13) to superimpose heat flux, all glazing windows indicate Q_h >0 and Q_c <0 during the heating and cooling period in cold zones, which are detrimental to indoor heating. During the heating period, TSGP exhibits the greatest Q while TAEP demonstrates the lowest Q during the cooling period, according to Equations (19) and (21), as well as Table 5. These two structures possess the most significant energy-saving potential in their respective heating and cooling processes. The energy-saving rate of TPAG is the second highest, at 30.25%. However, TAGP and TSGP feature external insulation, which has resulted in energy savings of 24.52% and 23.40%, respectively. Based on energy-saving rates alone, TAEP seems to be the optimal option for cold zones. However, based on the findings presented in Figure 9a–c, it is evident that the thermal performance of TAEP is inferior to TPGA's, owing to its lower liquid phase rate. This, in turn, could have negative implications on the quality of light and visibility during heating periods. Considering both energy efficiency and thermal performance, TPGA is the most optimal choice for application in cold zones.

Table 5. Q passing through the glazing windows in Beijing (cold zones).

	DP	TAGP	TAEP	TPGA	TSGP
Heating Q (kJ/m^2)	3464.93	4175.58	2426.92	4082.15	4897.79
Cooling Q (kJ/m^2)	27,324.67	21,795.87	16,803.50	21,333.99	22,835.91
$Q_{Eq.19}$ (kJ/m^2)	1,657,418.09	1,151,240.48	983,408.12	1,127,443.87	1,142,896.12

3.3. Hot Summer and Cold Winter Zone

Considering the requirement for both winter heating and summer cooling in Wuhan, it is important to account for the energy consumption of heat during both heating and cooling periods. As depicted in Figure 10a, the environmental conditions outside Wuhan on 19 February were chosen to simulate data, with a daily average temperature of 279.9 K and maximum solar radiation of 916 J/m^2. The daylight lasts from 8 a.m. until 6 p.m. The indoor temperature was set at 291.15 K. And the environmental conditions outside in Wuhan on 7 July were chosen to simulate the data, with a daily average temperature of 300.3 K and maximum solar radiation of 844 J/m^2. The daylight lasts from 7 a.m. until 8 p.m. The indoor temperature was set at 299.15 K.

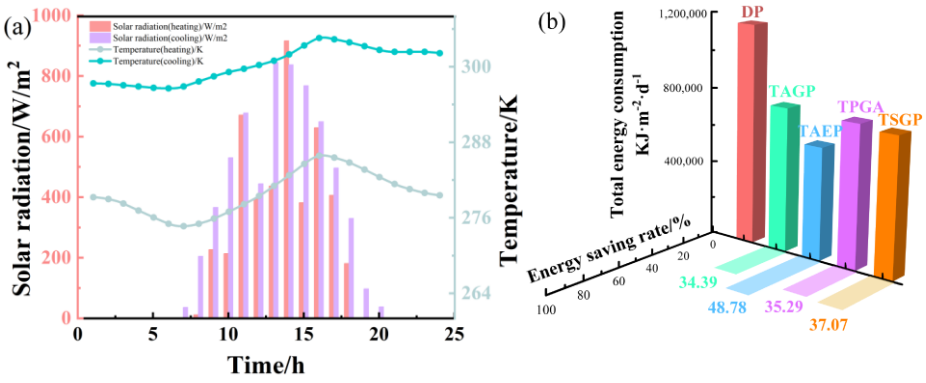

Figure 10. (**a**) Hourly values of air temperature and solar radiation in Wuhan; (**b**) Total energy consumption and energy-saving rate.

Figure 11a–c and (1–3) depict trends in the liquid phase rate of the PCM layer, the temperature, and the heat flux on the inner surface of glazing windows during the heating and cooling periods, respectively. As depicted in Figure 11a, the liquefaction rates of the PCM layers in DP and TPGA both reached 1. The complete liquefaction time for DP lasts 1 h, with a phase transition process occurring from 11:00 to 18:00, while for TPGA, it lasts 4 h with a phase transition process from 11:00 to 19:00. Specifically, adding insulation inside DP can extend the liquid time of PCM layers during the heating period in hot summer and cold winter zones. The liquefaction rate of TAGP and TSGP when insulated on the outside of DP is similar, except for the fact that the liquefaction time of TSGP is 1 h longer than TAGP's, indicating that silica insulation is marginally more effective compared to an air layer. For TAEP, the liquefaction rate of the PCM is the slowest, reaching a maximum of only 0.50, and the low-e glass reflects some of the solar radiation, hindering absorption by the PCM layer. Figure 11b suggests that the inner surface temperatures of both DP and TPGA exhibit a similar trend, as observed in the other structures with exterior insulation installed on DP. The highest inner surface temperature across all structures occurred at 15:00, with TPGA recording the lowest maximum internal surface temperature at 313.58 K. Notably, it is the most uniform and nearest to indoor comfort temperature when compared with other structures. From Figure 11c, the heat flux trend from the inner surface remains consistent among all structures, with TAEP displaying the mildest heat flux.

The energy consumption during the cooling period should also be analyzed, taking into account the climatic characteristics of hot summer and cold winter zones, as well as the occupants' needs for a comfortable indoor thermal environment. From Figure 11(1), all glazing windows experienced complete liquefaction of PCM layers, exhibiting a cooling period trend observed in cold zones. Some minor variations are observed due to the slightly higher outdoor temperatures in hot summer and cold winter zones. The complete liquefaction time for DP lasts from 10:00 to 19:00 for 10 h; for TAGP, TAEP, TSGP, it lasts from 11:00 to 19:00 for 9 h, while for TPGA, it lasts from 10:00 to 20:00 for 11 h. From Figure 11(2), it can be seen that the inner surface temperatures of DP and TPGA peaked at 16:00, with the highest peaks of 302.83 K for DP and 301.11 K for TPGA. Furthermore, the peak time for the inner surface temperatures of TAGP, TAEP, and TSGP are all delayed by 1 h compared to DP, with peaks reaching 300.77 K, 300.17 K, and 300.79 K, respectively, indicating that adding insulation can reduce peak temperatures during the cooling period in this region. Adding on the outer side can delay the time to reach the peak. The type of insulation added has little effect on the peak on the inside surface, and if the low-e glass is continued to be added on top of it, it can further reduce the peak. As shown in Figure 11(3), the heat flux through each glazing window follows a similar trend, with TAEP having the smoothest pattern.

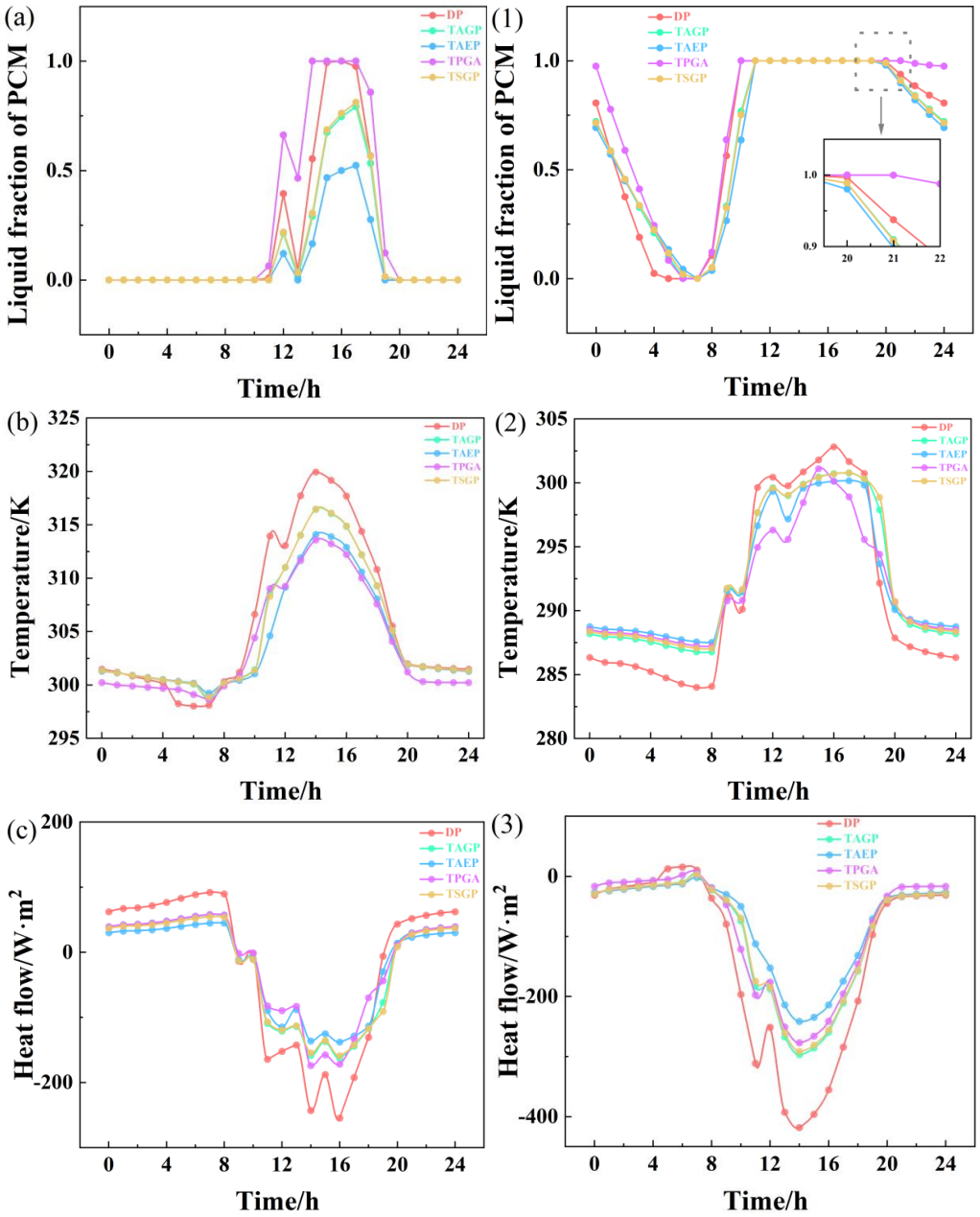

Figure 11. Thermal performance and energy efficiency of five glazing windows in hot summer and cold winter zone: Heating periodin hot summer and cold winter zone: (**a**) Average liquid fraction of PCM; (**b**) Average inner surface temperature; (**c**) Inside surface heat flow. Cooling period: (**1**) Average liquid fraction of PCM; (**2**) Average inner surface temperature; (**3**) Inner surface heat flow.

Referring to Equations (12) and (13), the combined heat flux on typical days results in $Q_h < 0$ and $Q_c < 0$ for all glazing windows during heating and cooling periods, respectively. The above result indicates that glazing windows are effective for heating but less optimal for cooling. Table 3 shows that Wuhan has 121 heating days and 123 cooling days. Equation (18) and Table 6 demonstrate that DP has the highest energy yield, which is the perfect fit for this region in the heating period. TAEP is the most energy-efficient structure with the lowest Q during the cooling period. It highlights that TAEP allows for the least amount of total energy consumption. The energy-saving potential of each glazing window in hot summer and cold winter zones is calculated using Equation (21), and the highest TAEP energy-saving rate is calculated to be 48.78%. TPGA has a slightly lower energy-saving rate of 30.25%, followed by TAGP and TSGP with a rate of 24.52% and 23.40%, respectively.

Table 6. *Q* passing through the glazing windows in Wuhan (hot summer and cold winter zones).

	DP	TAGP	TAEP	TPGA	TSGP
Heating *Q* (kJ/(m^2·d))	11,603.80	9727.57	6329.18	10,193.08	10,501.51
Cooling *Q* (kJ/(m^2·d))	27,019.94	21,347.48	14,587.94	20,912.04	22,284.34
$Q_{Eq.19}$ (kJ/m^2)	1,919,393.59	1,448,711.51	1,028,485.88	1,338,818.61	1,470,291.68

Considering only the energy-saving potential, the application of TAEP results in the greatest reduction in energy consumption for indoor heating. In zones with hot summer and cold winter, installing insulation on the interior of DP shows greater potential for energy-saving compared to adding insulation on the exterior. The type of insulation used on the exterior has minimal impact on the energy performance of PCM glazing windows. However, when further taking the impact on fluctuations of the indoor thermal environment into account, TPGA has the least impact, and the possibility of TPGA being the optimal solution can be considered.

3.4. Hot Summer and Warm Winter Zone

In Guangzhou, the demand for cooling energy is significantly greater than heating energy due to the hot summer and cold winter. As shown in Figure 12, the environmental conditions outside Guangzhou on 19 September were chosen to simulate the data, with a daily average temperature of 301.02 K and maximum solar radiation of 955 J/m^2. The daylight lasts from 9 a.m. until 8 p.m., and its indoor temperature was set at 299.15 K.

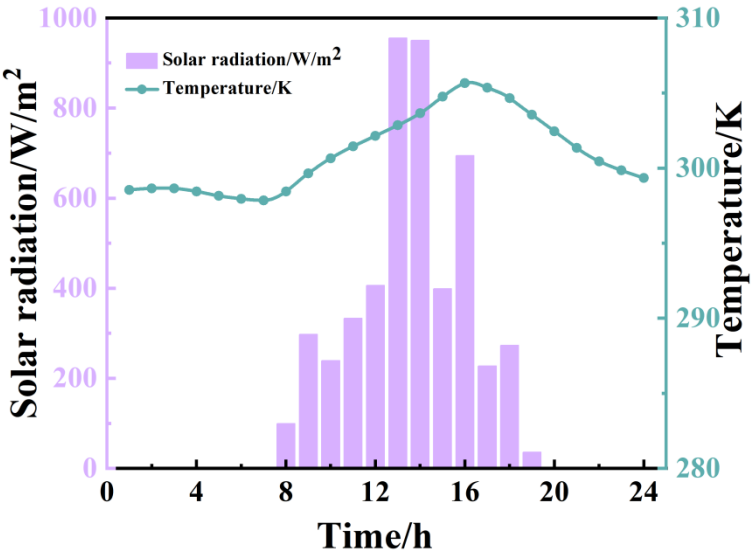

Figure 12. Hourly values of air temperature and solar radiation in Guangzhou.

Figure 13a–c depicts trends in the liquid fraction of PCM layers, the temperature, and the heat flux on the inner surface of glazing windows, respectively. As illustrated in Figure 13a, DP takes approximately 2 h for complete liquefaction, while both TAGP and TSGP take 1 h, and TPGA takes up to 6 h for complete liquefaction. it implies that applying inner insulation of DP causes the PCM layer to overheat, and its presence limits heat dissipation to the interior, resulting in the TPGA's PCM layer remaining in a liquid state for a longer period than DP's. As depicted in Figure 13b, DP and TPGA reach a maximum inner surface temperature at 15:00, whereas TAEP, TAGP, and TSGP experience a delay before reaching their maximum internal surface temperature, which indicates that adding exterior insulation to DP during the cooling period in hot summer and warm winter zones can effectively delay the peak inner surface temperature. As can be seen in Table 7, TAEP exhibits the lowest peak temperature of 311.56 K, with a flatter trend as compared to

the other structures. And TAEP has the smallest difference between the peak and the valley of the interior surface temperature (15.87 K), which shows the minimal impact of TAEP on the fluctuation of the indoor temperature. This is due to the effectiveness of the low-e glass in reflecting solar radiation and preventing overheating by the PCM layer. As illustrated in Figure 13c, the heat flux trends on the inner surfaces of all structures are relatively consistent, with DP experiencing the most dramatic maximum heat flux of -418.62 W/m^2. TAEP has the smoothest maximum heat flow of -201.74 W/m^2. Based on the above analysis, it is evident that TAEP minimizes the impact on indoor temperature fluctuations.

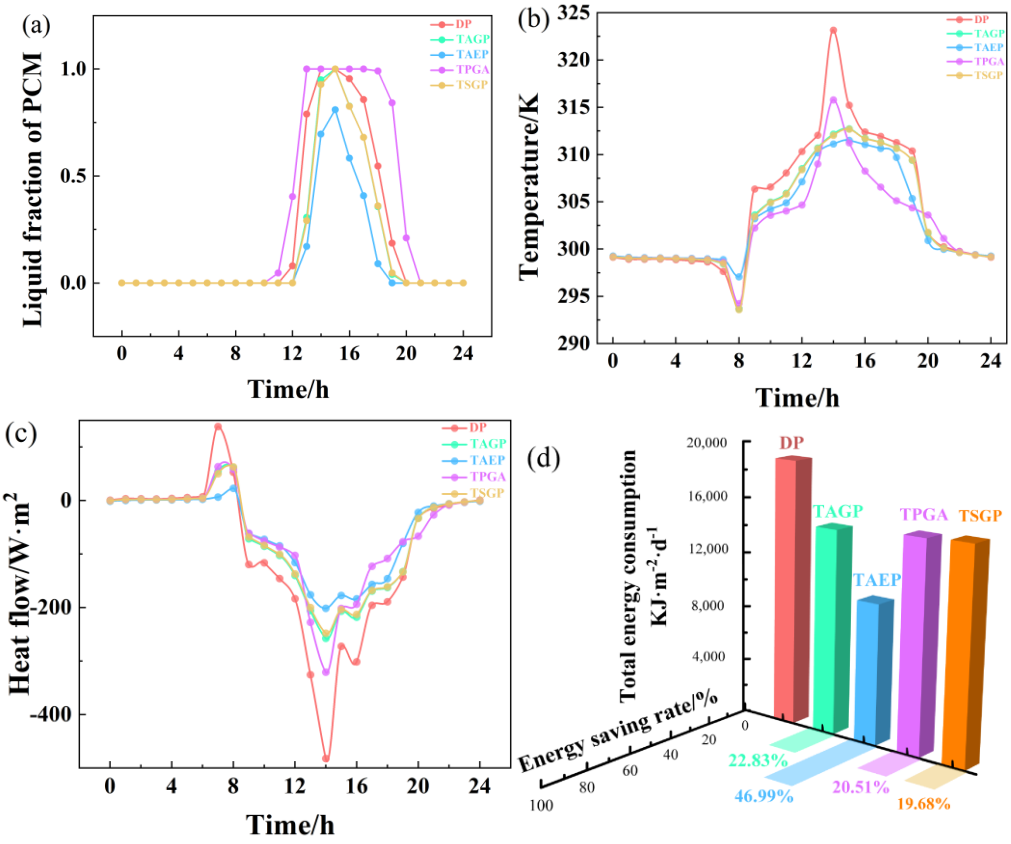

Figure 13. Thermal performance and energy efficiency of five glazing windows in hot summer and warm winter zone: (**a**) Average liquid fraction of PCM; (**b**) Average inner surface temperature; (**c**) Inner surface heat flow; (**d**) Total heat loss and energy-saving rate.

Table 7. Interior surface temperatures of different glazing windows and total energy entering the room through the glazing windows in Guangzhou (hot summer and warm winter zones).

Glazing Window	Peak Value T_{max} (K)	Peak Time (h)	Valley Value T_{min} (K)	ΔT (K) = $T_{max} - T_{min}$	Average Value (K)	Q (kJ/(m^2·d))
DP	323.16	14.00	282.94	40.22	304.45	19,056.73
TAGP	314.70	14.03	289.44	25.26	303.54	14,706.41
TAEP	311.56	14.52	295.70	15.87	303.24	10,101.16
TPGA	315.79	14.55	291.65	24.15	302.62	15,147.30
TSGP	314.37	14.73	289.66	24.70	303.52	15,306.98

Equation (13) reveals that Q_c <0 for all structures during the cooling period in hot summer and warm winter zones. As shown in Table 7 and Figure 13d, for the cooling period during hot summer and warm winter zones, the thermal performances of five PCM glazing windows are analyzed, and TAEP is found to exhibit the highest energy efficiency with an energy-saving of 46.99%. The energy efficiency using TAGP, TPGA,

and TSGP is 22.38%, 20.51%, and 19.68%, respectively, according to Equation (21); the energy efficiency of TSGP with silica aerogel added to the outer pane is not only inferior to TSGP featuring an air layer on the exterior but also to TSGP possessing an air layer on the interior. Thus, TSGP is unsuitable for hot summer and warm winter zones. The maximum heat energy entering the room through DP is 19,056.73 kJ/(m^2·d), while the TAEP is 10,101.16 kJ/(m^2·d), representing the lowest amount of heat entering the room from the outside. The use of TAEP can greatly reduce building cooling energy consumption. Consider the following, TAEP can be considered the most suitable for optimized glazing windows in hot summer and warm winter zones. It combines energy-saving potential with minimal impact on indoor thermal comfort. In hot summers and warm winter zones. TAEP is the best optimization strategy for DP in hot summer and warm winter zones.

3.5. Mild Zone

The amount of energy used for heating in Kunming is significantly greater than that used for cooling, a result of the mild climate in the zone. Therefore, only the heating energy consumption has been taken into account. As depicted in Figure 14, the environmental conditions outside Kunming on the 28th of the month were chosen to simulate the data, with a daily average temperature of 283.04 K and maximum solar radiation of 803 J/m^2. The daylight lasts from 10 a.m. until 8 p.m. The indoor temperature was set at 291.15 K.

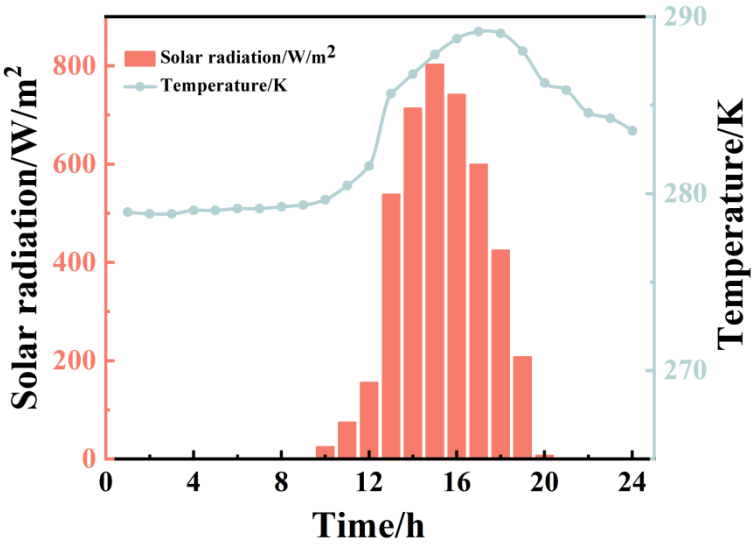

Figure 14. Hourly values of air temperature and solar radiation in Kunming.

Figure 15a–c illustrates the trends in the liquid fraction of PCM layers, the temperature, and the heat flux on the inner surface of glazing windows, respectively. As depicted in Figure 15a, DP and TPGA achieved complete liquefaction in roughly 4h, while TAGP and TSGP both achieved complete liquefaction in 1 h. As depicted in Figure 15b and Table 8, all of the combination glazing windows exhibit a delayed peak temperature by 1 h. These findings suggest that adding insulation to the outer pane of DP during the heating period in mild zones can effectively delay the peak temperature of the inner surface of glazing windows. TAEP records the lowest temperature fluctuation (12.54 K) and exhibits a temperature trend that is the flattest and closest to the indoor comfort level compared to all other structures. Figure 15c shows that the inner surface heat flux trends for DP and TPGA are identical, while those for TAEP, TAGP, and TSGP are more moderate. The analysis suggests that adding insulation to the outer pane is more appropriate for maintaining a stable indoor thermal environment during the heating period in mild zones.

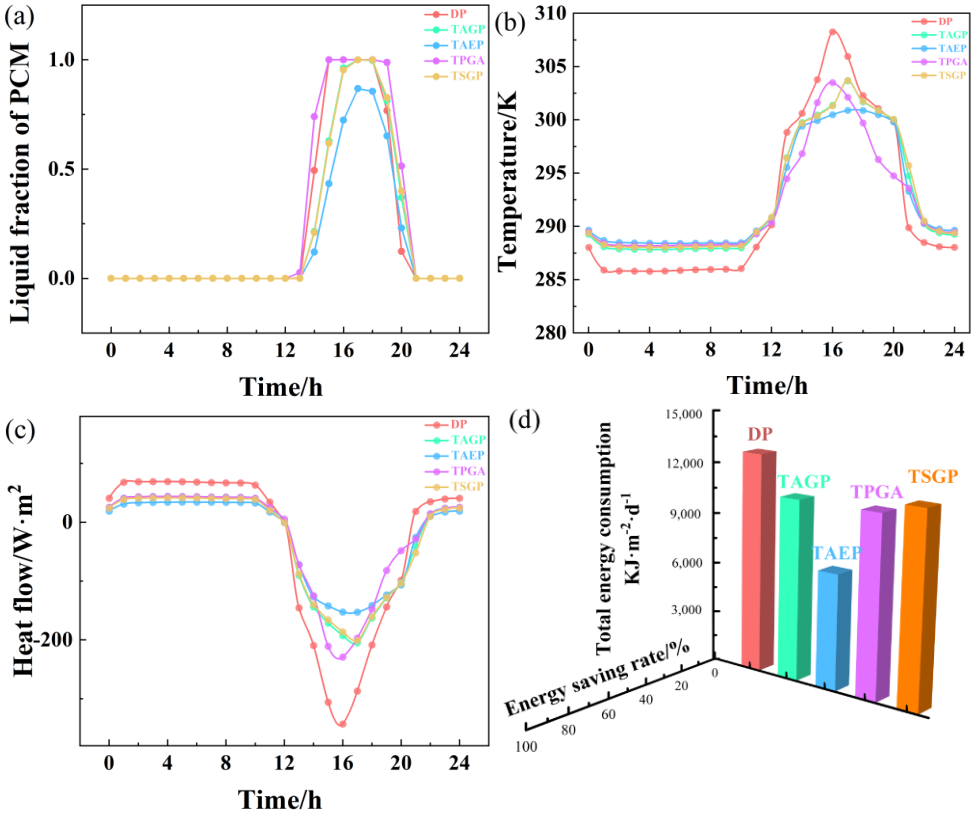

Figure 15. Thermal performance and energy efficiency of five glazing windows in mild zone: (**a**) Average liquid fraction of PCM; (**b**) Average inner surface temperature; (**c**) Inner surface heat flow; (**d**) Total heat loss and energy-saving rate.

Table 8. Interior surface temperatures of different glazing windows and total energy entering the room through the glazing windows in Kunming (mild zones).

Glazing Window	Peak Value T_{max} (K)	Peak Time (h)	Valley Value T_{min} (K)	ΔT (K) = $T_{max} - T_{min}$	Average Value (K)	Q (kJ/(m^2·d))
DP	308.29	15.88	285.78	22.51	292.11	12,829.52
TAGP	303.70	16.85	287.83	15.88	292.83	10,596.22
TAEP	300.95	16.48	288.40	12.54	292.75	6809.96
TPGA	303.50	15.92	288.18	15.32	292.24	10,655.70
TSGP	303.72	16.90	288.03	15.69	292.97	11,314.18

When $Q_h < 0$ according to Equation (12), it indicates that heat is transferred from outdoors to indoors. This is advantageous for building heating, and Q is calculated using Equation (16) during the heating period. Table 8 and Figure 15d highlight that DP allowed the highest amount of heat energy to enter the room at 12,829.52 KJ/(m^2·d), which is most beneficial during the heating period in mild zones. All the other structures show lower levels of heat gain compared to DP, with TAEP having at least 6019.56 kJ/(m^2·d) less heat gain than DP and being the least suitable for the heating period in mild zones. The heat gains of TSGP, TAGP, and TPGA are 11,314.18 kJ/(m^2·d), 10,596.21 kJ/(m^2·d), and 10,655.70 kJ/(m^2·d), respectively, with similar magnitudes, indicating that there is no discernible difference in energy efficiency between adding an air layer to the exterior and interior of DP during heating periods in mild zones. It is attributed to the unique climate conditions in mild zones, where there is minimal contrast between indoor and outdoor temperatures during the heating period and intense solar radiation. Therefore, the energy transferred by the temperature difference of glazing windows is negligible when compared to the effect of solar-transmitted radiant energy on a building's energy consumption. The

application of DP, which transmits the most solar radiant energy, is particularly beneficial for mild zones.

4. Conclusions

Double-layer PCM glazing windows (DP) and four multilayer glazing windows (TAGP, TAEP, TPGA, and TSGP) are proposed. Moreover, the thermal performance and energy-saving potential are numerically evaluated in different climates, respectively. The main conclusions are as follows:

When the heating demand is considered, the largest energy-saving rate appears in TSGP to be 40.28% in severe cold zones, and DP possesses the lowest energy consumption in mild zones. TAEP has maximized energy efficiency in hot summer and warm winter zones with high cooling demand, having an energy-saving rate of 46.99%. For cold zones and hot summer and cold winter zones, both the heating and cooling demands are considered, TAEP offers the greatest energy-saving rates of 40.67% and 46.42%, respectively.

Compared to TAEP, TAGP exhibits lower energy-saving rates of 13.98% in cold zones, 14.39% in hot summer and cold winter zones, and 24.16% in hot summer and warm winter zones. TAEP in zones where cooling demand is the main consideration that can greatly reduce energy consumption.

TAGP is 19.96% less energy efficient than TSGP in severe cold zones, 3.18% in cold zones, and 2.15% in hot summer and cold winter zones. Conversely, TAGP is 19.96% more 3.15% energy efficient than TSGP in hot summer and warm winter zones. TSGP is more suitable for zones with heating needs compared to TAGP.

TPGA is 11.64% less energy efficient than TAGP in cold zones and is 2.32% in hot summer and warm winter zones. In cold zones and hot summer and cold winter zones, there is not much difference in the energy-saving rates. TAGP is designed to be more energy efficient than TPGA.

In cold severe zones, the recommended optimization strategy for TSGP is DP. In cold zones, hot summer and cold winter zones, and hot summer and warm winter zones, TAEP is deemed as an optimization strategy for DP. In mild zones, multilayer composite structures with DP are not advisable.

Additional low-e coating is the most efficient choice to reduce fluctuations of temperature and heat flux on the inner surface of the glazing window.

The current work provides the optimization strategies of multilayer combination structures of DP in various climate zones in China through numerical simulation analyses. However, in this paper, the investigation of the PCM glazing windows is conducted over a typical day to represent the entire heating or cooling period, a long-term study is necessary for our forthcoming research to assess its practical application implications. The evolution of sustainable technologies for energy utilization and saving are essential issue that needs to be addressed [49]. The examination and evaluation of optimization strategy for multilayer PCM-glazed structures across diverse climate zones could extend the implementation of PCM glazing windows in various areas, thus accelerating the development of sustainable development construction.

Author Contributions: Idea for the article, Y.L. and Y.M.; Conceptualization, W.H. and F.K.A.; Methodology, C.Z. and Y.M.; Literature search, X.Y. and R.Y.; Data analysis, Z.Q. and D.L.; Draft of the work, Y.L. and M.K.; Revision of the work, D.L. and M.K.; Supervision, W.H. and F.K.A.; Project administration, Z.Q.; Funding acquisition, F.K.A. and D.L. All authors have read and agreed to the published version of the manuscript.

Funding: This work was funded by the Deanship of Scientific Research at the University of Bisha, grant number (UB-GRP-36-1444). The APC was funded by this grant. Financial support is provided by the National Science Foundation of China [52078110].

Institutional Review Board Statement: Not applicable.

Informed Consent Statement: Not applicable.

Data Availability Statement: Data are contained within the article.

Acknowledgments: The authors extend their appreciation to the Deanship of Scientific Research at the University of Bisha for funding this research through the general research project under grant number (UB-GRP-36-1444). Thankfulness is attributed to the National Science Foundation of China through the support grants [52078110].

Conflicts of Interest: The authors declare no conflict of interest.

Nomenclature

λ	thermal conductivity, W/(m·K)
c_p	specific heat, J/(kg·K)
ρ	density, kg/m^3
n	refractive index, -
α	absorption coefficient, 1/m
α_s/α_l	solid absorption coefficient and liquid absorption coefficient of PCM, 1/m
Q_L	latent heat, kJ/kg
τ	transmittance, -
ϕ	source term from solar radiation
I	solar radiation energy of the selected typical day, W/m^2
I_{out}	total radiation heat flux from the outside boundary to the ambient, W/m^2
I_a	heat radiation flux from the outside boundary to atmosphere, W/m^2
I_s	heat radiation flux from the outside boundary to sky, W/m^2
I_g	heat radiation flux from the outside boundary to ground, W/m^2
I_{in}	total radiation heat flux from the inside boundary to the indoor ambient, W/m^2
$q_{i,h}$	inner surface heat flux of each time step during heating period, kJ/(m^2·d)
$q_{i,c}$	inner surface heat flux of each time step during cooling period, kJ/(m^2·d)
d_m	thickness of each layer, m
E_τ	transmitted energy in solar radiation, kJ/m^2
$\omega_{i,j}$	interface reflectance, -
φ	fraction of liquid present, -
t	temperature, K
t_0	standard temperature, K
t_m	initial melting temperature, K
t_s	initial solidification temperature, K
t_{out}	outside boundary temperature, K
t_e	outdoor environment temperature, K
t_{in}	inside boundary temperature, K
$t_{e,i}$	indoor environment temperature, K
h_0	heat transfer coefficient on outside boundary, W/(m^2·K)
h_i	heat transfer coefficient on inside boundary, W/(m^2·K)
σ	Stefan Boltzmann constant, W/(m^2·K^4)
ε	surface emissivity of external glass layer, -
Q_h	cumulative hourly heat of heating period, kJ/(m^2·d)
Q_c	cumulative hourly heat of cooling period, kJ/(m^2·d)
Q	total heat gain through glazing windows, kJ/m^2
Q_D	heat through the double-glazing PCM windows, kJ/m^2
Q_M	heat through the multilayer PCM glazing windows, kJ/m^2
D_h/D_c	numbers of days during heating and cooling period, d
r	energy-saving rate, -

References

1. Alabid, J.; Bennadji, A.; Seddiki, M. A review on the energy retrofit policies and improvements of the uk existing buildings, challenges and benefits. *Renew. Sustain. Energy Rev.* **2022**, *159*, 112161. [CrossRef]
2. Fan, Y.; Xia, X. Energy-efficiency building retrofit planning for green building compliance. *Build. Environ.* **2018**, *136*, 312–321. [CrossRef]
3. Freire, R.Z.; Mazuroski, W.; Abadie, M.O.; Mendes, N. Capacitive effect on the heat transfer through building glazing systems. *Appl. Energy* **2011**, *88*, 4310–4319. [CrossRef]

4. Aritra, G. Diffuse transmission dominant smart and advanced windows for less energy-hungry building: A review. *J. Build. Eng.* **2023**, *64*, 105604.
5. Ghosh, A.; Norton, B. Advances in switchable and highly insulating autonomous (self-powered) glazing systems for adaptive low energy buildings. *Renew. Energy* **2018**, *126*, 1003–1031. [CrossRef]
6. Moran, P.; O'Connell, J.; Goggins, J. Sustainable energy efficiency retrofits as residenial buildings move towards nearly zero energy building (nzeb) standards. *Energy Build.* **2020**, *211*, 109816. [CrossRef]
7. Suresh, C.; Hotta, T.K.; Saha, S.K. Phase change material incorporation techniques in building envelopes for enhancing the building thermal comfort-a review. *Energy Build.* **2022**, *268*, 112225. [CrossRef]
8. Márta, Q.A. Experimental study of pcm-enhanced building envelope towards energy-saving and decarbonisation in a severe hot climate. *Energy Build.* **2023**, *279*, 112680.
9. Guo, J.; Zou, B.; Wang, Y.; Jiang, Y. Space heating performance of novel ventilated mortar blocks integrated with phase change material for floor heating. *Build. Environ.* **2020**, *185*, 107175. [CrossRef]
10. Al-Absi, Z.A.; Hafizal MI, M.; Ismail, M. Experimental study on the thermal performance of pcm-based panels developed for exterior finishes of building walls. *J. Build. Eng.* **2022**, *52*, 104379. [CrossRef]
11. Hu, J.; Yu, X.B. Adaptive building roof by coupling thermochromic material and phase change material: Energy performance under different climate conditions. *Constr. Build. Mater.* **2020**, *262*, 120481. [CrossRef]
12. Pielichowska, K.; Pielichowski, K. Phase change materials for thermal energy storage. *Prog. Mater. Sci.* **2014**, *65*, 67–123. [CrossRef]
13. Rathore, P.K.S.; Gupta, N.K.; Yadav, D.; Shukla, S.K.; Kaul, S. Thermal performance of the building envelope integrated with phase change material for thermal energy storage: An updated review. *Sustain. Cities Soc.* **2022**, *79*, 103690. [CrossRef]
14. Wieprzkowicz, A.; Heim, D. Modelling of thermal processes in a glazing structure with temperature dependent optical properties—An example of pcm-window. *Renew. Energy* **2020**, *160*, 653–662. [CrossRef]
15. Li, S.; Zou, K.; Sun, G.; Zhang, X. Simulation research on the dynamic thermal performance of a novel triple-glazed window filled with pcm. *Sustain. Cities Soc.* **2018**, *40*, 266–273. [CrossRef]
16. Silva, T.; Vicente, R.; Amaral, C.; Figueiredo, A. Thermal performance of a window shutter containing pcm: Numerical validation and experimental analysis. *Appl. Energy* **2016**, *179*, 64–84. [CrossRef]
17. Goia, F.; Perino, M.; Serra, V. Improving thermal comfort conditions by means of pcm glazing systems. *Energy Build.* **2013**, *60*, 442–452. [CrossRef]
18. Goia, F.; Perino, M.; Serra, V. Experimental analysis of the energy performance of a full-scale pcm glazing prototype. *Sol. Energy* **2014**, *100*, 217–233. [CrossRef]
19. Bolteya, A.M.; Elsayad, M.A.; Belal, A.M. Thermal efficiency of PCM filled double glazing units in Egypt. *Ain Shams Eng. J.* **2021**, *12*, 1523–1534. [CrossRef]
20. Liu, C.; Bian, J.; Zhang, G.; Li, D.; Liu, X. Influence of optical parameters on thermal and optical performance of multi-layer glazed roof filled with pcm. *Appl. Therm. Eng. Des. Proc. Equip. Econ.* **2018**, *134*, 615–625. [CrossRef]
21. Arranz, B.; Ruiz-Valero, L.; Gonzlez, M.; Snchez, S. Comprehensive experimental assessment of an industrialized modular innovative active glazing and heat recovery system. *Energy* **2020**, *212*, 118748. [CrossRef]
22. Li, S.; Sun, G.; Zou, K.; Zhang, X. Experimental research on the dynamic thermal performance of a novel triple-pane building window filled with pcm. *Sustain. Cities Soc.* **2016**, *27*, 15–22. [CrossRef]
23. Berthou, Y.; Biwole, P.H.; Achard, P.; Sallee, H.; Tantot-Neirac, M.; Jay, F. Full scale experimentation on a new translucent passive solar wall combining silica aerogels and phase change materials. *Sol. Energy* **2015**, *115*, 733–742. [CrossRef]
24. Souayfane, F.; Biwole, P.H.; Fardoun, F. Thermal behavior of a translucent superinsulated latent heat energy storage wall in summertime. *Appl. Energy* **2018**, *217*, 390–408. [CrossRef]
25. Hamzat, A.K.; Omisanya, M.I.; Sahin, A.Z.; Oyetunji, O.R.; Olaitan, N.A. Application of nanofluid in solar energy harvesting devices: A comprehensive review. *Energy Convers. Manag.* **2022**, *266*, 115790. [CrossRef]
26. Moghaieb, H.S.; Padmanaban, D.B.; Kumar, P.; Haq, A.U.; Maddi, C.; McGlynn, R.; Mariotti, D. Efficient solar-thermal energy conversion with surfactant-free cu-oxide nanofluids. *Nano Energy* **2023**, *108*, 108112. [CrossRef]
27. Li, Z.R.; Hu, N.; Fan, L.W. Nanocomposite phase change materials for high-performance thermal energy storage: A critical review. *Energy Storage Mater.* **2023**, *55*, 727–753. [CrossRef]
28. Li, D.; Yang, R.; Arc, M.; Wang, B.; Tunbilek, E.; Wu, Y.; Liu, C.; Ma, Z.; Ma, Y. Incorporating phase change materials into glazing units for building applications: Current progress and challenges. *Appl. Therm. Eng.* **2022**, *210*, 118374. [CrossRef]
29. Karlessi, T.; Santamouris, M.; Synnefa, A.; Assimakopoulos, D.; Didaskalopoulos, P.; Apostolakis, K. Development and testing of pcm doped cool colored coatings to mitigate urban heat island and cool buildings. *Build. Environ.* **2011**, *46*, 570–576. [CrossRef]
30. Lei, J.; Kumarasamy, K.; Zingre, K.T.; Yang, J.; Wan, M.P.; Yang, E.H. Cool colored coating and phase change materials as complementary cooling strategies for building cooling load reduction in tropics. *Appl. Energy* **2017**, *190*, 57–63. [CrossRef]
31. Ji, R.; Li, X. Numerical analysis on the energy performance of the pcms-integrated thermochromic coating building envelopes. *Build. Environ.* **2023**, *233*, 110113. [CrossRef]
32. Zhou, Y.; Zheng, S. Climate adaptive optimal design of an aerogel glazing system with the integration of a heuristic teaching-learning-based algorithm in machine learning-based optimization. *Renew. Energy* **2020**, *153*, 110113. [CrossRef]
33. Synnefa, A.; Santamouris, M.; Akbari, H. Estimating the effect of using cool coatings on energy loads and thermal comfort in residential buildings in various climatic conditions—Sciencedirect. *Energy Build.* **2007**, *39*, 1167–1174. [CrossRef]

34. Li, C.; Wen, X.; Cai, W.; Wu, J.; Shao, J.; Yang, Y.; Wang, M. Energy performance of buildings with composite phase-change material wallboards in different climatic zones of china. *Energy Build.* **2022**, *273*, 112398. [CrossRef]
35. Wang, P.; Liu, Z.; Zhang, X.; Zhang, H.; Chen, X.; Zhang, L. Adaptive building roof combining variable transparency shape-stabilized phase change material: Application potential and adaptability in different climate zones. *Build. Environ.* **2022**, *222*, 109436. [CrossRef]
36. Buratti, C.; Belloni, E.; Merli, F.; Zinzi, M. Aerogel glazing systems for building applications: A review. *Energy Build.* **2020**, *231*, 110587. [CrossRef]
37. Zheng, D.; Chen, Y.; Liu, Y.; Li, Y.; Zheng, S.; Lu, B. Experimental comparisons on optical and thermal performance between aerogel glazed skylight and double glazed skylight under real climate condition. *Energy Build.* **2020**, *222*, 110028. [CrossRef]
38. Chen, Y.; Xiao, Y.; Zheng, S.; Liu, Y.; Li, Y. Dynamic heat transfer model and applicability evaluation of aerogel glazing system in various climates of china. *Energy* **2018**, *163*, 1115–1124. [CrossRef]
39. Jelle, B.P.; Kalnaes, S.E.; Gao, T. Low-emissivity materials for building applications: A state-of-the-art review and future research perspectives. *Energy Build.* **2015**, *96*, 329–356. [CrossRef]
40. Zhang, S.; Ma, Y.; Li, D.; Liu, C.; Yang, R. Thermal performance of a reversible multiple-glazing roof filled with two pcm. *Renew. Energy* **2022**, *182*, 1080–1093. [CrossRef]
41. *GB50176-1993*; Code for the Thermal Design of Civil Buildings. China Ministry of Construction: Beijing, China, 1993.
42. *GBT50176-2016*; Thermal Design Code for Civil Building. China Building Publishing House: Beijing, China, 2016.
43. Available online: https://energyplus.net/ (accessed on 26 October 2023).
44. Zhang, G.; Wang, Z.; Li, D.; Wu, Y.; Arıcı, M. Seasonal thermal performance analysis of glazed window filled with paraffin including various nanoparticles. *Int. J. Energy Res.* **2020**, *44*, 3008–3019. [CrossRef]
45. Goia, F.; Perino, M.; Haase, M. A numerical model to evaluate the thermal behaviour of PCM glazing system configurations. *Energy Build.* **2012**, *54*, 141–153. [CrossRef]
46. Ismail, K.A.R.; Salinas, C.T.; Henriquez, J.R. Comparison between PCM filled glass windows and absorbing gas filled windows. *Energy Build.* **2008**, *40*, 710–719. [CrossRef]
47. Wang, F.; Shuai, Y.; Tan, H.; Lin, R.; Cheng, P. Researches on a new type of solar surface cladding reactor with concentration quartz window. *Sol. Energy* **2013**, *94*, 177–181. [CrossRef]
48. Li, D.; Wu, Y.; Liu, C.; Zhang, G. Energy investigation of glazed windows containing nano-pcm in different seasons. *Energy Convers. Manag.* **2018**, *172*, 119–128. [CrossRef]
49. Yang, C.; Wu, H.; Cai, M.; Zhou, Y.; Guo, C.; Han, Y.; Zhang, L. Valorization of Biomass-Derived Polymers to Functional Biochar Materials for Supercapacitor Applications via Pyrolysis: Advances and Perspectives. *Polymers* **2023**, *15*, 2741. [CrossRef]